Journal of Applied Electrochemistry **32**: 1053–1056, 2002.

Short communication

Synthesis and electrochemical performance of layered $Li[Li_{(1-2x)/3}Ni_xMn_{(2-x)/3}]O_2$ cathode materials for lithium secondary batteries

Y-K. SUN[1,*], S-S. SHIN[1] and I-H. OH[2]
[1]*Department of Chemical Engineering, Hanyang University, Seungdong-Gu, Seoul 133-791, Korea*
[2]*Division of Chemical Engineering, Korea Institute of Science and Technology, PO Box 131, Cheongryang-RT, Seoul 130-650, Korea*
*(*author for correspondence, e-mail: yksun@hanyang.ac.kr)*

Received 20 March 2002; accepted in revised form 20 June 2002

Key words: layered materials, lithium secondary batteries, manganese oxides, sol–gel method, solid solution

1. Introduction

Presently, commercial lithium-ion batteries use the $LiCoO_2$ cathode which has a well-ordered layered crystal structure and gives reversible and fast lithium extraction/insertion. Because of the high cost and toxicity of cobalt, an intensive search for new cathode materials has been underway over the past decade. Manganese oxides are lower cost, abundant, non-toxic, and safer on overcharge compared with $LiCoO_2$. However, the spinel $Li_{1+x}Mn_{2-x}O_4$, which is the most readily prepared among manganese oxides, suffer from solubility problems at elevated temperatures [1,2]. The search for layered $LiMnO_2$ with the same structure as $LiCoO_2$ is being pursued, but the materials tend to transform to the more stable spinel phase during electrochemical cycling due to the Jahn–Teller ions of Mn^{3+} [3–6]. The ideal cathode material will combine the superior electrochemical performance such as high capacity, good rate capability and long cycle life with low cost and environmental acceptability.

Recently, the stabilization of layered structures by using solid solutions between Li_2MnO_3 and $LiMO_2$ (M = Cr, Ni, Co) such as $Li[Li_{(1-2x)/3}Ni_xMn_{(2-x)/3}]O_2$ and $Li[Li_{(1-x)/3}Co(Cr)_xMn_{(2-2x)/3}]O_2$ have been studied. [7–10]. Li_2MnO_3 has a layered structure similar to $LiCoO_2$, $LiNiO_2$ and $LiCrO_2$. In Li_2MnO_3 and $LiMO_2$ solid solution, M is the redox-active species, while tetravalent manganese in $Li_{1/3}Mn_{2/3}$ clusters is electrochemically inactive [11]. It has been reported that the electrochemical capacity results from oxidation of Cr^{3+} to Cr^{6+}, Ni^{2+} to Ni^{4+} and Co^{3+} to Co^{4+} in $Li[Li_{(1-x)/3}Cr_xMn_{(2-2x)/3}]O_2$, $Li[Li_{(1-2x)/3}Ni_xMn_{(2-x)/3}]O_2$, and $Li[Li_{(1-x)/3}Co_xMn_{(2-2x)/3}]O_2$, respectively.

In this paper, we report the synthesis and electrochemical properties of $Li[Li_{(1-2x)/3}Ni_xMn_{(2-x)/3}]O_2$ (x = 0.35, 0.305 and 0.23) materials.

2. Experimental details

$Li[Li_{(1-2x)/3}Ni_xMn_{(2-x)/3}]O_2$ (x = 0.35, 0.305 and 0.23) powders were prepared by a sol–gel method using glycolic acid as a chelating agent. $Li(CH_3COO)\cdot 2H_2O$ (Kanto Chemical Co.), $Ni(CH_3COO)_2\cdot 4H_2O$ (Aldrich Chemical Co.), and $Mn(CH_3COO)_2\cdot 4H_2O$ (Acros Organics) were dissolved in distilled water, and added dropwise to a continuously stirred aqueous solution of glycolic acid (Kanto Chemical Co.). A pH of the solution was adjusted to $8 \sim 8.5$ using ammonium hydroxide. The resultant solution was evaporated at $70 \sim 80$ °C until a transparent sol and gel was obtained. The resulting gel precursors were decomposed at 450 °C for 10 h in air and then thoroughly ground using a mortar and pestle. The obtained powders was pressed into pellets, heated at 900 °C for 3 h in air, and then quenched to room temperature.

Powder X-ray diffraction (Rigaku, Rint-2000) using CuK_α radiation was used to identify the crystalline phase of the as-prepared powders and cycled electrodes. Rietveld refinement was then performed on the X-ray diffraction data to obtain lattice constants.

Charge–discharge cycles were performed in CR2032 coin type cells. The cell consisted of a cathode and a lithium metal anode separated by a porous polypropylene film. For the fabrication of the electrode, the mixture, which contained 20 mg $Li[Li_{(1-2x)/3}Ni_xMn_{(2-x)/3}]O_2$ powders and 12 mg conducting binder (8 mg of teflonized acetylene black (TAB) and 4 mg of graphite), was pressed on 2.0 cm^2 stainless screen at 800 kg cm^{-2}. The used electrolyte was a 1:2 mixture of ethylene carbonate (EC) and dimethyl carbonate (DMC) containing 1 M $LiPF_6$ by volume. The charge–discharge cycling was carried out galvanostatically at a current rate of 0.4 mA cm^{-2} (40 mA g^{-1}) between 2.5 and 4.6 V at 30 °C.

3. Results and discussion

Figure 1 shows X-ray diffraction patterns of $Li[Li_{(1-2x)/3}Ni_xMn_{(2-x)/3}]O_2$ (x = 0.35, 0.305 and 0.23) powders. Although we cannot specifically identify the crystal structure of the materials, all of the diffraction

peaks could be indexed to a hexagonal α-$NaFeO_2$ structure with space group *R3m*. The XRD patterns of the materials show a single phase of layered structure and are quite narrow indicating good crystallinity of the materials. As can be seen in Figure 1, a hexagonal phase judging from the more splitting of (1 0 8) and (1 1 0) peaks increased and diffraction peaks characteristic for Li_2MnO_3 (monoclinic phase) at 20–25° increased with increasing Li concentration in $Li[Li_{(1-2x)/3}Ni_x$-$Mn_{(2-x)/3}]O_2$. However, no decrease in the ratio of the (0 0 3)/(1 0 4) diffraction peak was observed with increasing Li content, which implies no disordering Li, Ni and Mn cations in the transition metal layer (3b site). The lattice parameters (*a* and *c*) of the materials increase with increasing Ni concentration in $Li[Li_{(1-2x)/3}$-$Ni_xMn_{(2-x)/3}]O_2$ implying that Ni^{2+} ($r^{2+}_{Ni} = 0.69$ Å) ions could be substituted for Li^+ ($r^{+}_{Li} = 0.76$ Å) and Mn^{4+} ($r^{4+}_{Mn} = 0.53$ Å) ions; The lattice parameters of $Li[Li_{0.1}Ni_{0.35}Mn_{0.55}]O_2$ and $Li[Li_{0.18}Ni_{0.23}$-$Mn_{0.59}]O_2$ are *a* of 2.872 and 2.863 Å, and *c* of 14.269 and 14.259 Å, respectively.

The typical voltage profiles of $Li/Li[Li_{(1-2x)/3}$-$Ni_xMn_{(2-x)/3}]O_2$ ($x = 0.35$, 0.305 and 0.23) cells for the 10th cycle are shown in Figure 2. The $Li/Li[Li_{(1-2x)/3}$-$Ni_xMn_{(2-x)/3}]O_2$ cells display smooth, monotonous charge–discharge curves and exhibit similar voltage profile reported by other researchers [7–10]. Although all samples prepared have a smooth and monotonic voltage profile, the voltage shape of the $x = 0.23$ in $Li[Li_{(1-2x)/3}Ni_xMn_{(2-x)/3}]O_2$ is different from others ($x = 0.35$, 0.305). As can be seen in the voltage profile in Figure 2(c), the plateau appears during the reduction process between 3.0 and 3.5 V. This is more clearly observed by the differential capacity vs. voltage profile in Figure 3. Unfortunately, it is not possible to explain the structural changes at present, but it is considered that the growth of peaks at near 3.3 V in the charge process is the reason for the increase in capacity with increase in cycle number and lithium content in $Li[Li_{(1-2x)/3}Ni_xMn_{(2-x)/3}]O_2$.

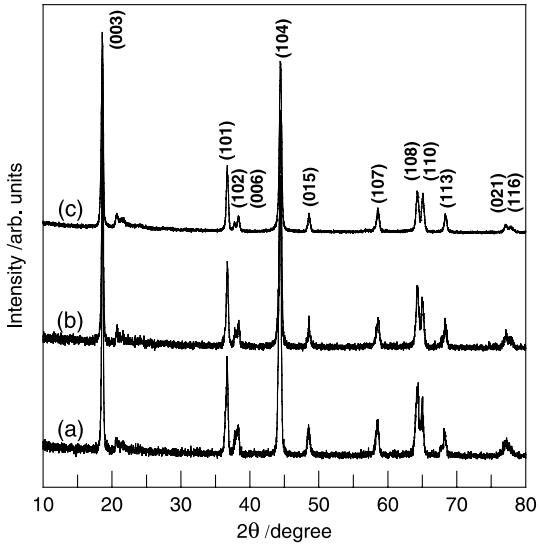

Fig. 1. X-ray diffraction patterns of $Li[Li_{(1-2x)/3}Ni_xMn_{(2-x)/3}]O_2$ (a) $x = 0.35$, (b) $x = 0.305$ and (c) $x = 0.23$ powders.

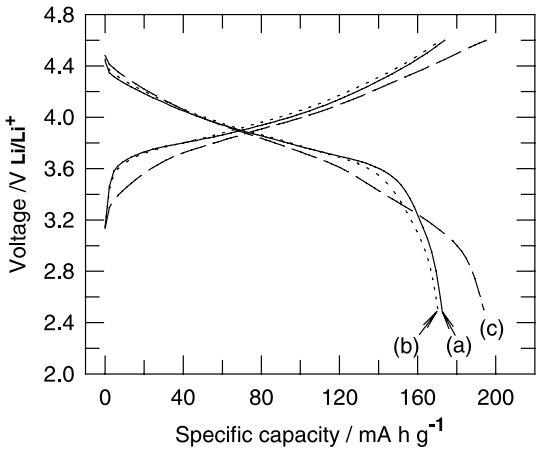

Fig. 2. 10th charge–discharge curves of $Li/Li[Li_{(1-2x)/3}Ni_xMn_{(2-x)/3}]$-$O_2$ cells (a) $x = 0.35$, (b) 0.305 and (c) 0.23 at a current density of 0.4 mA cm^{-2} in the voltages between 2.5 and 4.6 V.

Figure 4 shows the specific charge–discharge capacities of the $Li/Li[Li_{(1-2x)/3}Ni_xMn_{(2-x)/3}]O_2$ cell ($x = 0.35$, 0.305 and 0.23) as a function of cycle number at 30 °C. There is significant irreversible capacity loss of about 35 mA h g^{-1} on the first cycle for the three electrodes, which is about 20% of the first charge capacity. The discharge capacities of the three electrodes slowly increase during electrochemical cycling up to about the first 15 cycles and subsequently stabilize for further cycling. The $Li[Li_{(1-2x)/3}Ni_xMn_{(2-x)/3}]O_2$ electrodes with $x = 0.35$, 0.305 and 0.23 after the 15th cycle provide 173, 174 and 200 mA h g^{-1}, respectively. All the electrodes show excellent cyclability without capacity loss up to 40 cycles. The theoretical capacities of $Li[Li_{0.1}$-$Ni_{0.35}Mn_{0..55}]O_2$, $Li[Li_{0.13}Ni_{0.305}Mn_{0.565}]O_2$, and Li $[Li_{0.18}Ni_{0.235}Mn_{0.59}]O_2$ electrodes are 208, 184 and 146 mA h g^{-1}, respectively assuming that electrochemically active species is only Ni^{2+} ions and all the Ni^{2+} is oxidized to Ni^{4+} during lithium extraction/insertion. Considering the theoretical capacity of $Li[Li_{0.18}$-$Ni_{0.235}Mn_{0.59}]O_2$ electrodes, the delivered capacities of the materials is too high. It has been generally accepted that the charge compensation occurs at the M atoms (oxidation of M^{3+} to M^{4+}) while the oxygen valence is fixed at O^{2-} when Li^+ is extracted from the layered $LiMO_2$ (M = Co and Ni) structure. By contrast, based on recent research on oxygen valence change for $LiCoO_2$ [12–14], the oxygen valence also plays an important role for charge compensation, as well as Co ions. The oxygen charge state was not fixed constantly but changed gradually with lithium ion insertion/extraction, indicating that the oxygen ion contribute an electron exchange for charge compensation. It is also reported that the chemical state of oxygen was associated with the charge–discharge reaction of Li/Li-$Ni_xMn_{2-x}O_4$ cell and the formation of holes in the oxygen 2p orbital contributed to the capacity of 5 V in

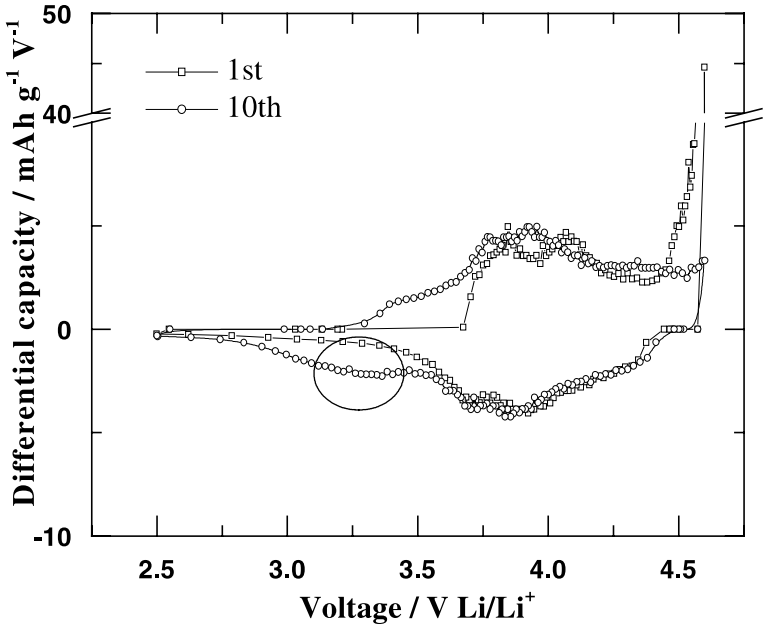

Fig. 3. Differential capacity against voltage of the $Li[Li_{(1-2x)/3}Ni_xMn_{(2-x)/3}]O_2$ ($x = 0.23$).

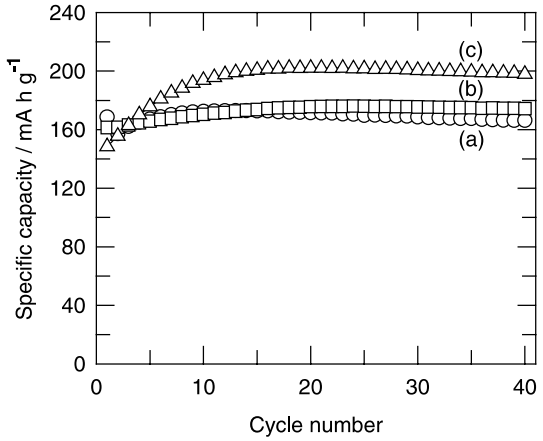

Fig. 4. Specific charge–discharge capacities of the $Li/Li[Li_{(1-2x)/3}Ni_xMn_{(2-x)/3}]O_2$ cells as a function of the cycle number at 30 °C. (a) $x = 0.35$, (b) $x = 0.305$, and (c) $x = 0.23$.

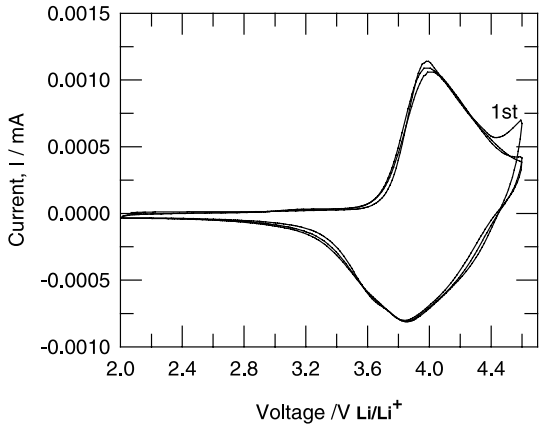

Fig. 5. Cyclic voltammogram of the $Li[Li_{(1-2x)/3}Ni_xMn_{(2-x)/3}]O_2$ electrode ($x = 0.305$) between 2.0 and 4.6 V at a scan rate of 100 μV s^{-1}.

spinel $LiNi_xMn_{2-x}O_4$ [15]. Although we still cannot explain the unusually large capacity and the key parameter governing the capacity of $Li[Li_{0.18}Ni_{0.235}Mn_{0.59}]O_2$, it is deliberated that the capacity of the materials partly results from the oxygen valence change.

Figure 5 shows cyclic voltammogram of the first three cycles of the $Li[Li_{0.13}Ni_{0.305}Mn_{0.565}]O_2$ electrode between 2.0 and 4.6 V at a scan rate of 100 μV s^{-1}. The important feature is the difference between the first and subsequent cycles. An oxidation peak appears at near 4.6 V in the first oxidation process, which may be related to the irreversible capacity loss is at first charging. On the subsequent cycle, the oxidation and reduction processes show only one peak centred at 4 and 3.85 V, respectively. This is consistent with the cyclic voltammogram data of the $Li[Li_{x/3}Mn_{2x/3}Co_{1-x}]O_2$ ($x = 0.1$) electrode composed of solid solution of $LiCoO_2$ and Li_2MnO_3 [7]. This behaviour implies that severe structural degradation is not expected during the lithium extraction/insertion process of $Li[Li_{0.13}Ni_{0.305}Mn_{0.565}]O_2$ electrode. Further study is now in progress to reveal the unusual large capacity and structural stability of $Li[Li_{x/3}Mn_{2x/3}Co_{1-x}]$ materials.

4. Conclusions

Layered $Li[Li_{(1-2x)/3}Ni_xMn_{(2-x)/3}]O_2$ ($x = 0.35$, 0.305 and 0.23) powders with high homogeneity and crystallinity have been synthesized using a sol–gel method. The layered structure solid solutions were obtained by Ni substitution for Li and Mn in Li_2MnO_3. The discharge capacity of the $Li[Li_{(1-2x)/3}Ni_xMn_{(2-x)/3}]O_2$ electrode increased with decrease in Ni concentration. The $Li[Li_{0.18}Ni_{0.235}Mn_{0.59}]O_2$ electrode delivers a very high capacity of 200 mA h g^{-1} with excellent cyclability.

Although the unusual capacity behaviour is not yet revealed, the oxygen valence may also play an important role for charge compensation in $Li[Li_{(1-2x)/3}Ni_xMn_{(2-x)/3}]O_2$ materials.

Acknowledgement

This work is supported in part by the Ministry of Information & Communication of Korea ('Support Project of University Information Technology Research Center' supervised by KIPA).

References

1. G.G. Amatucci, C.N. Schmutz, A. Bylr, C. Siala, A.S. Gozdz, D. Larcher and J-M. Tarascon, *J. Power Sources* **69** (1997) 11.
2. Y-K. Sun, D-W. Kim and Y-M. Choi, *J. Power Sources* **79** (1999) 231.
3. Y. Shao-Horn, S.A. Hackney, A.R. Armstrong, P.G. Bruce, R. Gitzendanner, C.S. Johnson and M.M. Thackeray, *J. Electrochem. Soc.* **146** (1999) 2404.
4. A.R. Armstrong, R. Gitzendanner, A.D. Robertson and P.G. Bruce, *Chem. Commun.* (1988) 1833.
5. Y-I. Jang, B. Huang, Y-M. Chiang and D.R. Sadoway, *Electrochem. Solid-State Lett.* **1** (1998) 13.
6. B. Ammundsen, J. Desilvestro, T. Groutso, D. Hassell, J.B. Metson, E. Regan, R. Steiner and P.J. Pickering, *J. Electrochem. Soc.* **147** (2000) 4078.
7. K. Numata, C. Sakaki and S. Yamanaka, *Solid State Ionics* **117** (1999) 257.
8. B. Ammundsen, J. Desilvestro, R. Steiner and P. Pickering, Tenth international meeting on 'Lithium Batteries', Vol 97–98, Como, Italy, 28 May–2 June (2000).
9. T. Ohzuku and Y. Makimura, *Chem. Lett.* (2001) 744.
10. Z. Lu, D.D. MacNeil and J.R. Dahn, *Electrochem. Solid-State Lett.* **4** (2001) A191.
11. B. Ammundsen and J. Paulsen, *Adv. Mater.* **13** (2001) 943.
12. G. Ceder, Y.M. Ching, D.R. Sadoway, M.K. Aydinol, Y.I. Jang and B. Huang, *Science* **392** (1998) 694.
13. L.A. Montoro, M. Abbate and J.M. Rosolen, *Electrochem. Solid-State Lett.* **3** (2000) 410.
14. J. Graetz, A. Hightower, C.C. Ahn, R. Yazami, P. Rez and B. Fultz, *J. Phys. Chem. B* **106** (2002) 1286.
15. Y. Uchimoto and T. Yao, Abstract 242, Tenth international meeting on 'Lithium Batteries', Como, Italy, 28 May–2 June, (2000).